A&A manuscript no.
(will be inserted by hand later)

Your thesaurus codes are:
09.01.1; 09.07.1; 09.13.2; 11.05.1; 11.09.1; 11.09.4;

ASTRONOMY
AND
ASTROPHYSICS
1.2.2008

Molecular absorption and its time variations in Cen A

T. Wiklind[1], **F. Combes**[2]

[1] Onsala Space Observatory, S–43992 Onsala, Sweden
[2] DEMIRM, Observatoire de Paris, 61 Av. de l'Observatoire, F–75014 Paris, France

Received date; Accepted date

Abstract. New high quality absorption spectra of J=1←0 HCO^+, HCN, HNC and the J=2←1 line of CS towards the center of the radio core of Cen A (NGC 5128) are presented. In addition the absorption profile of the J=1←0 line of $H^{13}CO^+$ has been detected for the first time, revealing that most absorption features have low opacities. The new HCO^+ spectrum allows a comparison with results obtained more than 7 years earlier. No significant change in the spectrum is found. From this remarkable result, constraints can be put on the minimum size of the radio source in the millimeter range (>500 AU). A comparison of abundance ratios between different absorption components suggests that the absorbing gas is essentially low density gas, with both low excitation and kinetic temperatures. Relative molecular abundances are compatible with those of the Milky Way. A parametrization of the high signal–to–noise spectrum of HCO^+ is presented for future reference when looking for spectral changes.

Key words: interstellar medium: molecules – galaxies: Cen A, ISM, absorption lines, radio continuum

1. Introduction

The nearby giant elliptical galaxy Cen A (NGC 5128) contains a warped disk of dust and dense gas. Optically the disk is seen as obscuration against a background of the old stellar population belonging to the elliptical galaxy. The presence of Hα emission in the disk (cf. Nicholson et al. 1992) suggest that formation of massive stars are currently taking place in the disk.

The disk is also a source of molecular line emission. Several studies have shown that it contains about $3 \times 10^8\,M_\odot$ of H_2. The distribution of the molecular gas has been traced by the CO emission (Eckart et al. 1990a, Quillen et al. 1992, Rydbeck et al. 1993, Wild et al. 1997). The emission extends to a galactocentric distance of approximately 1 kpc. The molecular gas distribution and its kinematics is consistent with a thin disk which is severly warped (Quillen et al. 1992). The main components are a ring or spiral arm at a galactocentric distance of ∼800 pc (adopting a distance of 3 Mpc to Cen A, which means that 1" corresponds to 14.5 pc.) and a circumnuclear ring at a radius of ∼100 pc (Israel et al. 1990, Rydbeck et al. 1993). The inner ring is seen as high velocity wings in spectra towards the center when the angular resolution is better than 25–30". It has also been imaged with the aid of deconvolution of single dish CO(2–1) data (Rydbeck et al. 1993). The inner ring is inclined relative to the outer disk but aligned perpendicular to the inner radio jet. The molecular gas properties of the disk appears to be similar to those found in normal spiral galaxies (cf. Israel et al. 1990, Eckart et al. 1990, Wild et al. 1997).

The radio core is hidden behind a large column of dense obscuring gas. The combination of a strong radio continuum source and a large column of dense gas makes the line of sight towards the center of Cen A a rich source of molecular absorption lines.

The properties of the gas seen in absorption is still largely unknown. Several studies have come up with conflicting results, both concerning the location of the absorption components relative to the nucleus as well as the temperature and density of the gas. The HI absorption towards the nucleus shows three absorption components; one strong at the systemic velocity around $552\,km\,s^{-1}$ and two redshifted ones at 596 and $609\,km\,s^{-1}$, respectively. Towards the inner jet, only the main absorption at $552\,km\,s^{-1}$ is seen (van der Hulst et al. 1983). This has been interpreted as evidence that the main $552\,km\,s^{-1}$ line is situated far out in the disk, while the redshifted lines are situated very close to the nucleus, possibly falling in to the center. However, Seaquist & Bell (1990) report a detection of redshifted H_2CO λ2cm absorption against the inner jet at a velocity of $\sim 576\,km\,s^{-1}$. This is not necessarily a proof against the redshifted component being situated close to the nucleus. The inner jet is seen at a projected distance of ∼20" from the core, which corresponds to ∼300 pc. The

Send offprint requests to: T. Wiklind, tommy@oso.chalmers.se

inner molecular disk can be extended on these scales (cf. Israel et al. 1991, Rydbeck et al. 1993, Hawarden et al. 1993). The molecular absorption lines seen in the millimeter range only occurs towards the radio core of Cen A, since the inner jet has a steep radio spectrum with a completely negligible continuum flux at mm wavelengths.

Molecular absorption lines seen in our Galaxy (cf. Lucas & Liszt 1996) and towards high redshift galaxies (Wiklind & Combes 1996ab, 1995, Combes & Wiklind 1996) almost exclusively arise in very cold gas (in terms of excitation temperature). Although the abundance ratio of HCN/HNC imply that the kinetic temperature can be in the range 10–20 K, the excitation temperature is comparable to the cosmic microwave background. This suggests diffuse gas with $n(H_2) < 10^3$ cm^{-3}. Are the molecular absorption lines seen in Cen A likewise coming from diffuse gas? Unfortunately very few multiline transitions of the same molecule have been observed. One exception is H_2CO, for which Seaquist & Bell (1990) derive an upper limit to the excitation temperature of 3.9 K. Several OH absorption features have been detected by van Langevelde et al. (1995), their interpretation is complicated by the presence of maser lines. Some come from diffuse gas, and some features point to dense clumps ($n(H_2) > 10^4$ cm^{-3}). The three lowest rotational lines of CO have been seen in absorption, both the lines around the systemic velocity and the redshifted components. The mere detection of the CO(3–2) line (cf. Israel et al. 1991) implies that the excitation temperature is relatively high (10–20 K). For CO, however, the analysis is complicated by confusion with emission, especially for the two lowest transitions.

In this paper we present new high quality observations of the HCO^+(1–0), HCN(1–0), HNC(1–0) and CS(2–1) absorption lines, as well as the previously unobserved $H^{13}CO^+$(1–0) transition, in order to shed some light on the physical properties and location of the molecular absorption towards the radio core of Cen A.

In Sect. 2 we present the observations, in Sect. 3 we identify the different absorption components and question their possible time variations and in Sect. 4 we derive column densities and abundance ratios. In Sect. 5 we discuss the implied properties of the absorbing gas in Cen A, and its assumed distance from the center.

2. Observations

The observations were done with the 15–m Swedish–ESO Submillimeterwave Telescope (SEST) at La Silla in Chile. The HCO^+, $H^{13}CO^+$ and N_2H^+ lines were observed in December 1995, the HCN, HNC and CS lines in July 1996, where we also obtained some additional observations of the HCO^+ and $H^{13}CO^+$ lines. A final observing session in August 1996 only involved the $H^{13}CO^+$ line.

For all the observations we used the 3–mm SIS mixer, giving a system temperature in the range 140–160 K at the observed frequencies (see Table 1). The low $T_{\rm sys}$ allowed us to obtain spectra with significantly better signal–to–noise than previous observations of the molecular absorption line system in Cen A. As backend we used the high resolution Acoustical Spectrometer (AOS), giving a resolution of 43 kHz or 0.14 km s^{-1}. Due to a Lorentzian response of the AOS, the actual velocity resolution of the spectra are slightly worse than this. The effective resolution is $\sim$0.2 km s^{-1}. The observations were done in a dual beam-switch mode, with a beamthrow of $\pm 11\farcm9$ in azimuth at a switchfrequency of 6 Hz. Both the receiver system and the weather were good and stable during the observations. The pointing was checked on the continuum of Cen A itself and the rms variations were less than 3". The good pointing accuracy is evident as small rms variations of the continuum level in 10 minute averages of spectra obtained during 8 hours of observations.

The observed continuum levels at the different frequencies are given in Table 1. Some of the high resolution spectra show a distinct curvature due to the presence of emission. We subtracted a second order baseline from the average spectra of each molecular line. Redshifted absorption features in the velocity range 560–640 km s^{-1} can be seen in the HCO^+, HCN, HNC and CS spectra. The region between 490–660 km s^{-1} was therefore omitted from the fitting procedure. The bandwidth of the spectrometer does not cover the full extent of the emission seen in low resolution data (cf. Israel et al. 1992). We derived the continuum level at the edges of the spectra in order to eliminate contribution from the emission. For HCO^+ and HCN, however, the presence of emission produces a flux $\lesssim$2% too high. This transforms into an error in the optical depth calculations which is 10% for the deepest HCO^+ absorption. For a line with a depth of 0.5 relative to the continuum, the error is <3%.

The 3–mm continuum flux decreased by $\sim$20% between December 1995 and July 1996. This is consistent with intrinsic variations of the millimetric flux of Cen A (cf. Tornikoski et al. 1996). The dispersion in the continuum flux determinations are caused by pointing and calibration errors. The latter is of the order 10%, whereas the former is likely to be less than this. The opacities of the absorption lines are, however, independent on the pointing[1], given only by the continuum to line ratio. In the following we have normalized all the continuum levels to unity using the fluxes given in Table 1. The continuum measured at λ3mm does get a contribution from the far-infrared dust emission in the disk. This is, however, insignificant. With a dust temperature of 36 K, as derived from the IRAS 60 and 100 μm fluxes, and a flux of 320.6 Jy at 100 μm, the contribution to the continuum at λ3mm is at most 2%. This is calculated assuming a dust emissivity $\propto \nu$. A more realistic dust emissivity ($\propto \nu^\alpha, \alpha > 1.0$) makes the dust emission negligble at λ3mm.

[1] This is true as long as the only contribution to changes in the observed continuum level is due to pointing offsets.

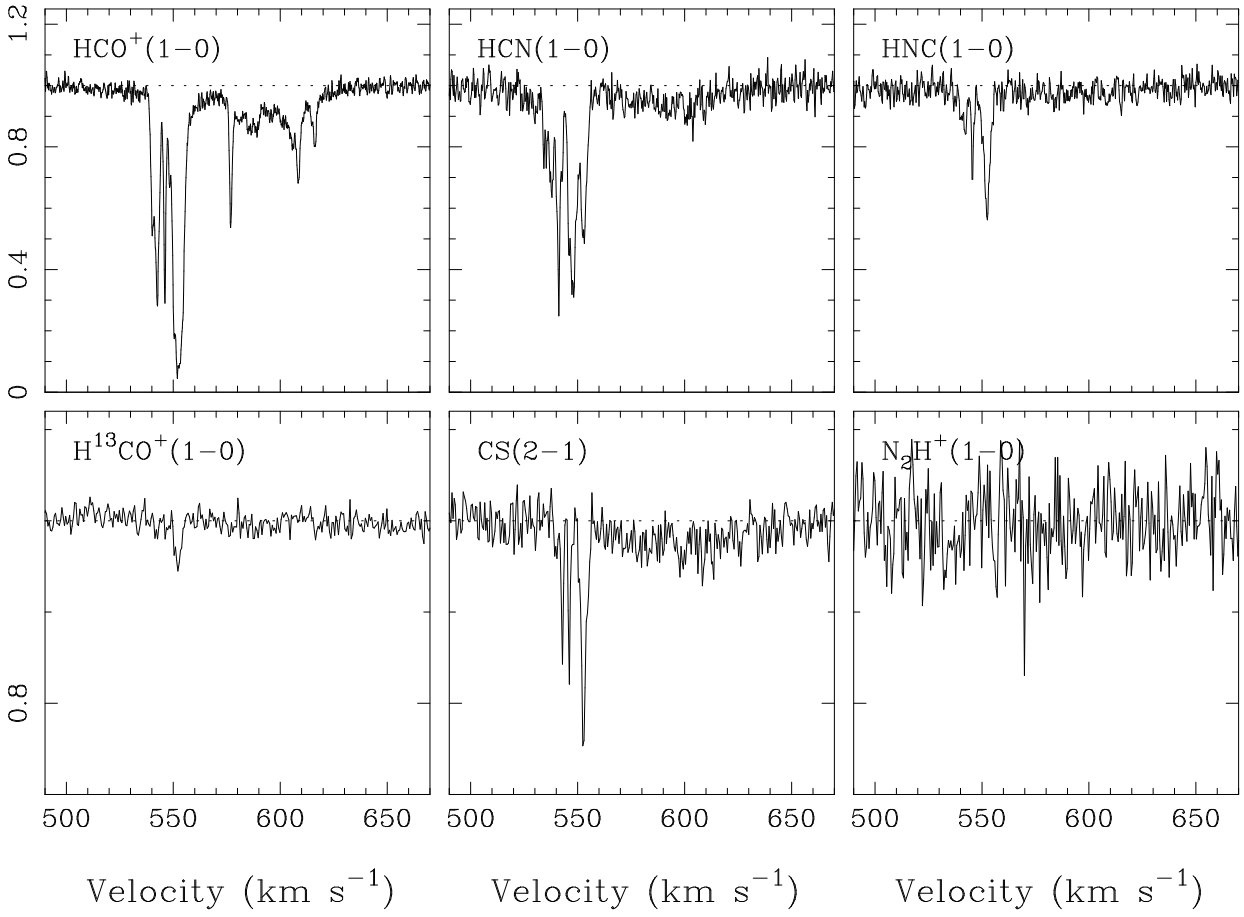

Fig. 1. Spectra of the observed transitions: HCO^+(1–0), $H^{13}CO^+$(1–0), HCN(1–0), HNC(1–0), CS(2–1) and N_2H^+(1–0). Only N_2H^+ remains undetected. The spectra have been normalized to a continuum level of unity. The velocity scale is heliocentric and the frequency definition is relativistic (see text). The velocity resolution is $0.2\,\mathrm{km\,s^{-1}}$ for HCO^+, $0.4\,\mathrm{km\,s^{-1}}$ for HCN, HNC and CS, and $0.6\,\mathrm{km\,s^{-1}}$ for $H^{13}CO^+$ and N_2H^+.

Table 1. Observed molecules

Molecule	Transition J⟶J–1	Frequency[a] GHz	T_{cont} mK[b]	Observing date
$H^{13}CO^+$	1–0	86.754294	409,355,308	Dec95, Jul96, Aug96
HCN	1–0	88.630415	320	Jul96
HCO^+	1–0	89.188518	410,340	Dec95, Jul96
HNC	1–0	90.663450	325	Jul96
N_2H^+	1–0	93.173500	314	Dec95
CS	2–1	97.980968	350	Jul96

a) The rest–frequency of the observed molecules (ν_0 in Eqs 1–2) taken from Lovas (1992).
b) In the T_{A}^* temperature scale. Conversion to Jansky: 25 Jy/K.

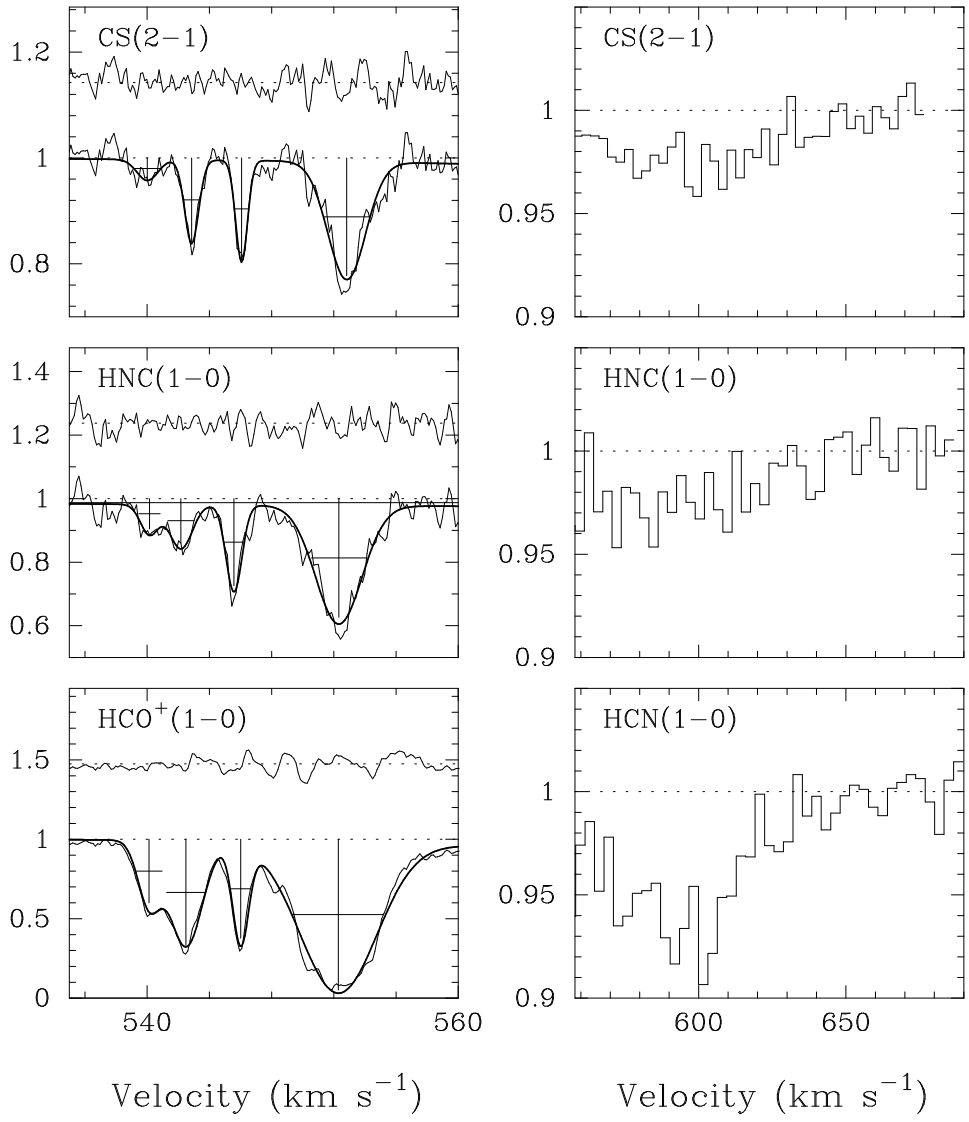

Fig. 2. The four main lines in the Low Velocity complex is shown to the left for CS(2–1), HNC(1–0) and HCO^+(1–0). Also shown are the results from a 5–component gaussfit. The residuals shown above the lines, are spectral values minus the fitted values. The fift component corresponds to the High Velocity complex, shown to the right. The HV complex has been binned to a velocity resolution of $3\,\mathrm{km\,s^{-1}}$. Notice the different scales. These five components define the main absorption lines (see Table 2).

The rest–frequencies of the observed molecules are given in Table 1. We used $v = 550\,\mathrm{km\,s^{-1}}$ as the systemic velocity for Cen A. All velocities are given as heliocentric with the relativistic definition of the frequency shift. This means that the center frequency of the spectrometer is given as

$$\nu_{\rm sky} \;=\; \nu_0\gamma\left(1-\frac{v}{c}\right) \quad \text{Relativistic}\,, \tag{1}$$

where v is the heliocentric velocity of the source (here $550\,\mathrm{km\,s^{-1}}$), c is the speed of light, ν_0 the rest-frequency as given in Table 1 and γ the Lorentz factor $1/\sqrt{1-v^2/c^2}$. The corresponding radio and optical definitions are

$$\begin{aligned} \nu_{\rm sky} \;&=\; \nu_0\left(1-\frac{v}{c}\right) \qquad \text{Radio} \\ \nu_{\rm sky} \;&=\; \nu_0\left(1+\frac{v}{c}\right)^{-1} \quad \text{Optical}\,. \end{aligned} \tag{2}$$

The observations in December were in fact done with the LSR velocity system and using the radio definition of the redshifted frequency. These observations have been shifted to a heliocentric velocity system and using the relativistic definition. In December 1995 $V_{\rm HEL} = V_{\rm LSR} - 2.208\,{\rm km\,s^{-1}}$. The velocity difference between the radio and relativistic frequency definitions amounts to $0.504\,{\rm km\,s^{-1}}$, with the relativistic definition giving a higher sky-frequency, i.e. the frequency to which the receiver is in effect tuned to. In order to convert the spectra obtained with the radio definition to the relativistic definition, we have to add $0.504\,{\rm km\,s^{-1}}$. Hence, the data obtained in December 1995 has been shifted by a total of $2.712\,{\rm km\,s^{-1}}$. Before adding the HCO^+ and $H^{13}CO^+$ obtained in December with that obtained in 1996, we mapped the 1995 spectra into the same channels as the 1996 spectra.

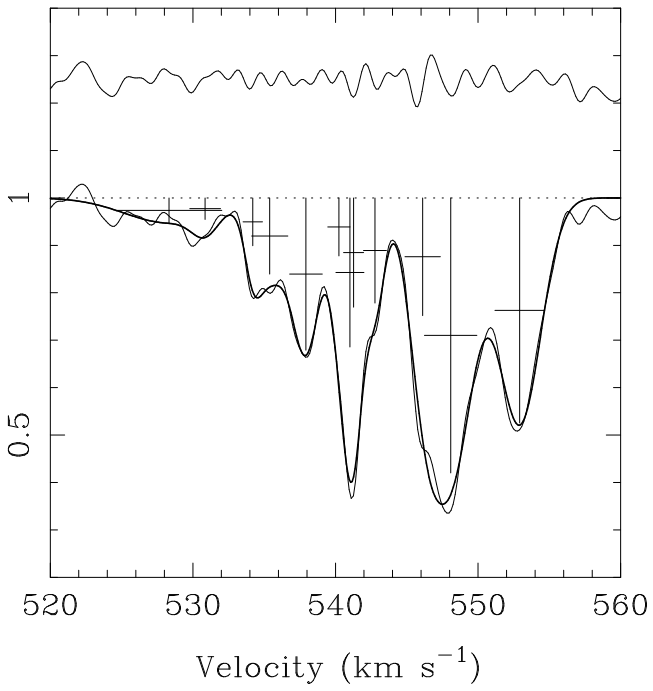

Fig. 3. Decomposition of the hyperfine components of HCN(1–0) in the LV complex. Four main absorption systems are assumed, each associated with three hyperfine lines of HCN. The center velocities of the components have been kept fixed in the fitting procedure.

3. Results

3.1. The spectra

The absorption spectra are shown in Fig. 1, with the continuum normalized to unity. The N_2H^+(1–0) line is not detected, despite the presence of an apparent line seen in Fig. 1. None of the 7 hyperfine components of this transition correspond to this line, moreover, its appearance differs from the lines detected in the other molecules. The N_2H^+ 'line' is an artefact caused by the receiver at this particular frequency. For HCO^+, HCN, HNC and CS we can identify two major absorption complexes.

– The strongest absorption feature is situated close to the systemic velocity of $552\,{\rm km\,s^{-1}}$, with a few relatively strong blue shifted absorption lines. We will henceforth call this complex of absorption lines the Low Velocity complex, or the LV complex. This complex consists of at least 4 different absorption components, extending between 540–556 $\,{\rm km\,s^{-1}}$. The high quality HCO^+ spectrum shows evidence for 7 components.
– Extended absorption at velocities redshifted relative to the systemic velocity is most evident in the HCO^+ line, but can be seen in the CS, HCN and HNC lines as well. We will refer to this complex as the High Velocity complex or the HV complex. The HV complex consists of a broad 'diffuse' absorption, extending from about $560\,{\rm km\,s^{-1}}$ to approximately $640\,{\rm km\,s^{-1}}$. The HCO^+ spectrum also shows several narrow absorption lines superposed on the broad absorption. These lines are absent from the other lines. The HV complex is not clearly evident in the $H^{13}CO^+$ spectrum shown in Fig. 1, but when binning the spectrum the HV complex is present at significant level of several sigma.

For reference we identify 5 main absorption lines, visible in all but the $H^{13}CO^+$ and N_2H^+ spectrum. No. 1–4 defines the LV complex and no. 5 is the broad diffuse HV complex. In Fig. 2 we show the LV and HV complexes in more detail. Superposed on the LV complex are the results of a 5–component gauss fit; four components for the LV complex and one for the HV complex (not shown). The fit parameters are given in Table 2. The residuals are similar to the rms noise level of the spectra, except for HCO^+, where the high signal–to–noise reveals the several additional unresolved components in the LV complex (of course, the HV complex of HCO^+ is poorly fitted by the fifth gauss component due to the presence of several narrow absorption lines). We will return to the HCO^+ spectrum in Sect. 3.3.

3.2. The hyperfine components of HCN

HCN is not part of Table 2 since each absorption system here consists of three hyperfine transitions. The high quality HCN(1–0) spectrum allows us to make a decomposition of the hyperfine lines by keeping the center velocities for each absorption system fixed at the value derived from the other molecules and only varying the intensity and width of the lines. The fitting is complicated by a near overlap of the F=0–1 hyperfine line of component 1 with the F=2–1 line of component 2. The fitting is not perfect and the results actually suggests the presence of at least a fifth component (adding three more hyperfine lines). However, with the present signal–to–noise ratio and overlap-

Table 2. Main gaussian components

	HCO^+(1–0)			$H^{13}CO^+$(1–0)			HNC(1–0)			CS(2–1)		
No.	$V_0^{a)}$ km s^{-1}	$T_0^{b)}$ mK	$\Delta V^{c)}$ km s^{-1}	$V_0^{a)}$ km s^{-1}	$T_0^{b)}$ mK	$\Delta V^{c)}$ km s^{-1}	$V_0^{a)}$ km s^{-1}	$T_0^{b)}$ mK	$\Delta V^{c)}$ km s^{-1}	$V_0^{a)}$ km s^{-1}	$T_0^{b)}$ mK	$\Delta V^{c)}$ km s^{-1}
4	540.12	399.7	1.68				540.15	94.8	1.37	540.01	39.7	1.58
3	542.49	668.3	2.48				542.17	139.2	1.70	542.86	158.2	1.07
2	546.01	622.5	1.22				545.58	273.9	1.20	546.07	192.3	0.90
1	552.29	948.3	5.84	552.16	50.1	3.03	552.32	373.0	3.50	552.83	221.5	2.86
5	593.94	139.5	50.12				575.65	25.5	101.04	596.79	28.6	62.59

a) Heliocentric velocity with relativistic velocity definition (see text).
b) Depth of the absorption line measured from the normalised continuum level (T_A^*).
c) Full width at half maximum depth.

Table 3. HCN(1–0) hyperfine components for the LV–complex$^{a)}$

	F= 1 − 1			F= 2 − 1			F= 0 − 1				
Comp.	Vel.$^{b)}$ km s^{-1}	T_{abs} mK	$\Delta V^{c)}$ km s^{-1}	Vel.$^{b)}$ km s^{-1}	T_{abs} mK	$\Delta V^{c)}$ km s^{-1}	Vel.$^{b)}$ km s^{-1}	T_{abs} mK	$\Delta V^{c)}$ km s^{-1}	$\int \tau_\nu dV$ km s^{-1}	$N^{d)}$ cm^{-2}
1	552.92	474	3.48	548.08	580	3.68	541.01	315	1.96	5.99	2.65×10^{13}
2	546.11	248	2.48	541.27	231	1.42	534.20	101	1.37	1.26	5.56×10^{12}
3	542.77	222	1.62	537.93	321	1.96	530.86	45:	2.16:	1.29	5.70×10^{12}
4	540.24	122	1.57	535.39	161	2.53	528.33	<55	7.3:	1.10	4.89×10^{12}

a) The absorption complex around the systemic velocity 553 km s^{-1}.
b) Heliocentric velocities with relativistic definition (see text).
c) Full width at half intensity.
d) Derived with an excitation temperature $T_x = 5$ K.

ping components, we use 4 absorption lines and smooth the HCN spectrum before fitting. The resulting decomposition is shown in Fig. 3 and the hyperfine components of the 4 main absorption lines in the LV complex is given in Table 3. The results are robust for all the F=1–0 lines and for all the F=2–1 lines, except for absorption line no. 2 which is situated within 0.3 km s^{-1} from the F=0–1 line of absorption line no. 1. The F=0–1 lines of line no. 3 and 4 are too weak to give completely reliable results. Nevertheless, the hyperfine line ratios, $R_{12} = I_{1-0}/I_{2-1}$ and $R_{02} = I_{0-1}/I_{2-1}$, as derived from the gaussian decomposition are given in Table 4.

3.3. Parametrization of the HCO$^+$ (1–0) spectrum

In order to facilitate future studies of the small scale structure of the molecular ISM along the line of sight towards the radio core in Cen A, we have parametrized the high quality HCO^+(1–0) absorption line shown in Fig. 1. The parametrization was done by fitting a number of gauss components to the spectrum. By starting out with a relatively small number of components and increasing the number until the residual does not show any large deviations from the rms noise of the spectrum, we found that a minimum of 17 components were needed. The reality of some of thes components should not be taken too seriously, since some absorption features may not be resolved and therefore do not show real gaussian profiles. The gaussian

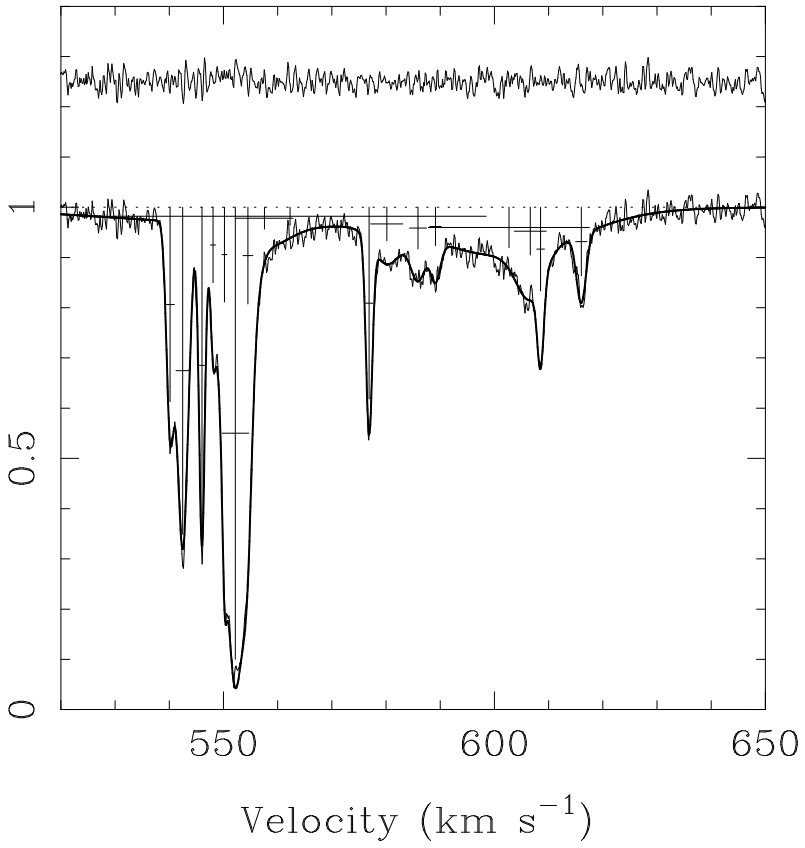

Fig. 4. Parametrization of the HCO^+(1–0) spectrum through a fit of 17 gaussian components. Data for the gaussian components are given in Table. 5. The residual is spectral value minus fitted value and has an rms similar to that of the original spectrum away from the absorption complexes. The velocity resolution is $0.2\,\mathrm{km\,s^{-1}}$.

Table 4. Ratios of HCN(1–0) hyperfine components for the LV–complex[a)]

	R_{12}		R_{01}	
Comp.	Peak[b)]	Integrated[c)]	Peak[b)]	Integrated[c)]
1	0.8	0.8	0.5	0.3
2	1.1	1.9	0.4	0.4
3	0.7	0.6	0.1	0.2
4	0.8	0.5	<0.3	<1.0

a) The absorption complex around the systemic velocity $553\,\mathrm{km\,s^{-1}}$.
b) Ratio of the peak anteanna temperatures.
c) Ratio of the component integrated intensity.

components can, however, be used for a precise representation of the absorption spectrum obtained by us and used for comparison with spectra obtained with different telescopes, spectrometers and spectral resolutions.

The gaussian components are given in Table 5 as the peak depth (measured from the normalized continuum), the full width at half intensity and the center velocity. The identification of these components are given from 1 to 17, and should not be confused by the identification of the 5 main absorption lines as given in Table 2. The HCO^+(1–0) spectrum with the fitted curve overlaid is shown in Fig. 4, together with a residual spectrum.

In addition to the HV and LV complexes there is an extended blueshifted absorption 'wing' in the HCO^+ spectrum. This is evident already in Fig. 4, but is more clearly seen in a smoothed spectrum. In Fig. 5 we show the HCO^+ spectrum binned to a velocity resolution of $2.1\,\mathrm{km\,s^{-1}}$. The blueshifted wing extends to about $500\,\mathrm{km\,s^{-1}}$. On the redshifted part of the spectrum, the broad absorption extends out to about $640\,\mathrm{km\,s^{-1}}$. In Fig. 6 we show the original data before baseline subtraction. The second order baseline which is subsequently used in the subtraction is shown as a dashed line. The peak of the baseline falls at $\sim$550 $\mathrm{km\,s^{-1}}$, as it should, despite the small and uneven regions where it was fitted. The depression at 500–

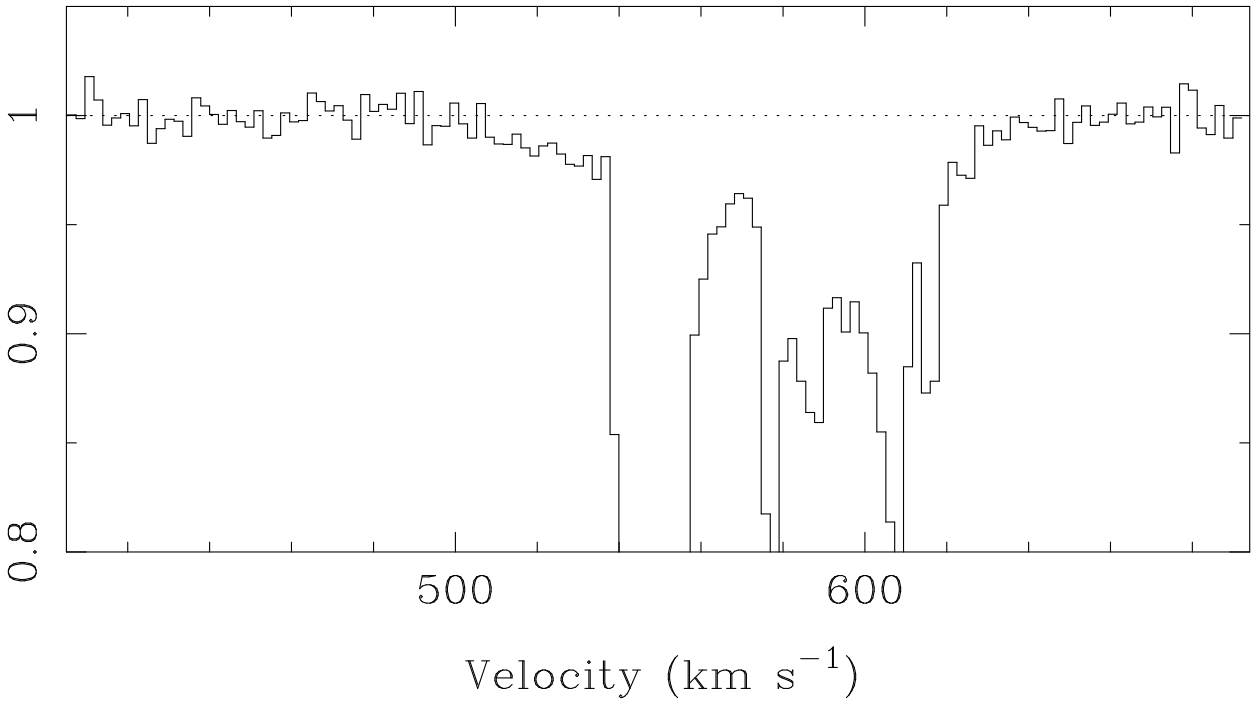

Fig. 5. The full extent of the HCO^+(1–0) spectrum. The data has been binned to give a velocity resolution of 2.1 km s^{-1}. The blueshifted absorption 'wing' extends to ∼500 km s^{-1}, while the absorption extends to ∼640 km s^{-1} on the redshifted side (see also Fig. 4).

540 km s^{-1} can be seen quite clearly. It is also present in the low resolution data presented by Israel (1992). Hence, the molecular absorption along the line of sight to the radio core in Cen A occurs continuously over 140 km s^{-1}. It is not possible to determine if the absorption in the range 500–540 km s^{-1} is a single blueshifted feature or if it is associated with the red 'wing' at ∼615–640 km s^{-1}.

3.4. Variations in the absorption lines?

The radio source in Cen A has a classical steep–spectrum double lobe structure, a steep–spectrum inner jet and a flat–spectrum core. VLBI observations at 8.4 GHz indicate that the core has a very small extent $\lesssim$2 milliarcseconds (mas) (Jones et al. 1996). The core is self absorbed at 2.3 GHz and brightens up to frequencies of ∼20 GHz. This small core is the likely source of the continuum emission seen at millimeter wavelengths. At a distance of 3 Mpc the extent of the core is thus only $\lesssim$0.03 pc, or 6000 AU. The core may even be considerably smaller; the variability at millimeter wavelengths observed by Kellerman (1974) suggests a size of the order a light day, or 175 AU. In addition to the core, a narrow steep–spectrum jet is conspicuous at 8.4 GHz (Jones et al. 1996); its intensity is already much weaker than the core, and will be completely negligible at mm wavelengths.

Small scale structure in the molecular ISM has been directly observed down to ∼2000 AU (e.g. Wilson & Walmsley 1989, Falgarone et al. 1992), while VLBI techniques allow detection of structures of 25 AU in the HI absorption medium in front of 3C radio sources (Diamond et al. 1989). Multi–epoch observations of 21cm absorption against high velocity pulsars also allowed detection of opacity variations of the ISM on a range of scales from 5 AU to 100 AU (Frail et al. 1994). In the molecular ISM, scales of the order of 10 AU have been inferred, through the time variations of H_2CO absorption lines (Marscher et al. 1993). Moore & Marscher (1995) confirmed these H_2CO absorption variations over a few years, in front of several point radio sources (3C111, NRAO150 and BL Lac). Through numerical simulations Marscher & Stone (1994) were able to derive constraints on the fractal structure of molecular clouds, from the time variability detections. The mean number of small clumps along the line of sight should be larger than previously thought, i.e. the size spectrum of clumps should be a steeper power–law, constraining the fractal dimension.

The surprising fact in these time variations of absorption features is that the involved gas appears to be diffuse. In the case of the 21cm absorption against pulsars, where small–scale opacity structures are detected towards *all* line of sights, the mean opacities are between 0.1 and 2.5, corresponding to N(HI) as low as $10^{19} - 10^{20}$ cm^{-2} (Frail et al. 1994). Also in the case of molecular 6cm H_2CO absorptions, the mean optical depth is very low (Moore & Marscher 1995). Of course variations of opaci-

Table 5. HCO^+(1–0) gaussian components

$HCO^+(1-0)$			
No.	$V_0^{a)}$ km s^{-1}	T_0 mK	$\Delta V^{b)}$ km s^{-1}
1	540.14	373.3	1.68
2	542.48	639.1	2.48
3	546.03	580.4	1.33
4	548.07	131.3	1.12
5	550.19	163.4	1.03
6	552.15	854.6	4.85
7	554.50	199.5	1.95
8	556.01	60.4	11.19
9	567.18	36.7	80.67
10	576.89	359.6	1.47
11	580.16	68.6	6.28
12	585.92	83.7	3.18
13	589.12	77.4	2.18
14	602.52	76.9	26.92
15	606.68	94.7	5.83
16	608.52	157.1	1.47
17	616.02	133.9	2.21

a) Heliocentric velocity with relativistic velocity definition (see text).
b) Full width at half minimum.

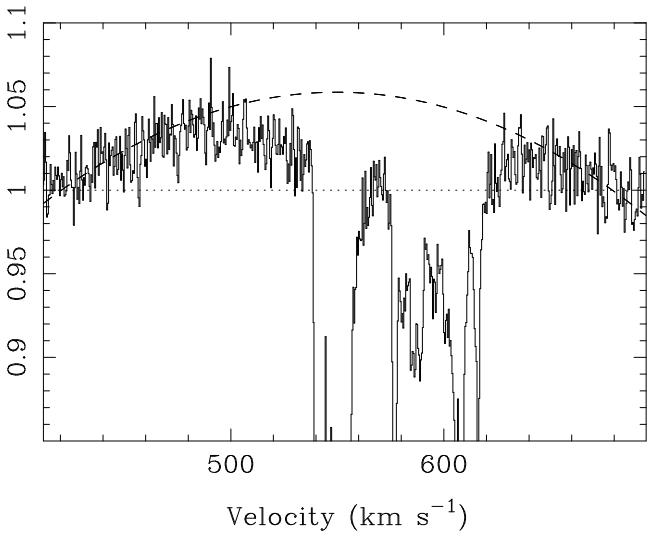

Fig. 6. The HCO^+(1–0) spectrum at a velocity resolution of 0.7 km s^{-1} before baseline removal. A second order baseline fit is shown as a dashed line. The blue 'wing' at 500–540 km s^{-1} is clearly visible.

ties are much more easy to detect when the opacity is low, since saturated profiles ($\tau >> 1$) are acutely sensitive to small variations in the noise level. But it was not expected to find contrasted small scale structures, and clumps, in such a diffuse gas. The opacity variations dectected are quite high (half of them have $\delta\tau > 0.1$, Frail et al. 1994), so they cannot be accounted for by mild density fluctuations. Clumps with density larger than $10^5 - 10^6$ cm^{-3} are implied (Moore & Marscher 1995). These clumps could represent 10–20% of the total column density.

The same physical conditions appear to be true for the molecular absorbing gas in front of the Cen A radio source. The opacities and column densities must be low in average, since the isotopic $H^{13}CO^+$ line is observed with about the expected abundance ratio with respect to the HCO^+ line. In these conditions, opacity variations should be easy to detect. The gaseous disk in Cen A has a rotational velocity of more than 250 km s^{-1}. The value is somewhat uncertain due to the strong warp of the disk and could be higher (cf. van Gorkom et al. 1990, Rydbeck et al. 1993). A rotational velocity of 250 km s^{-1} corresponds to a shift of the gas along the line of sight towards the radio core in Cen A by ∼50 AU per year.

The first molecular absorption line observations in Cen A was obtained in 1976 (Gardner & Whiteoak 1976), of formaldehyde. However, it wasn't until 1989 that the first high resolution molecular absorption line data was obtained, which can be used for a detailed comparison with the present data (cf. Eckart et al. 1990). Hence, the time span is about 7 years and a comparison with this data is thus sensitive to spatial scales in the ISM of 300–500 AU.

The HCO^+(1–0) spectrum published by Eckart et al. (1990) does not have as good signal–to–noise ratio as the current one and any comparison is limited by the rms noise in the 1989 data. In Fig. 7 we show our HCO^+(1–0) spectrum and the one obtained by Eckart et al. (1990) in 1989. Both spectra have been binned to a velocity resolution of 0.6 km s^{-1}. The lower panel in Fig. 7 shows the difference between the two spectra; 1995/96 − 1989 with equal weighting. A small residual feature can be seen in the difference spectrum at a velocity of 552 km s^{-1}, with a depth ∼10% of the normalized continuum level. This feature corresponds to the deepest absorption line. It could, however, be an effect of a slightly incorrect continuum flux in the 1989 data. If the continuum flux has been overestimated, the line–to–continuum ratio decreases (and the difference will show up for the strongest absorption feature). Likewise, an incorrect continuum level for the 1995/96 data could mimic the residual feature. The latter is not likely, since the observing conditions for the 1995/96 data were very good. Also, a comparison between the HCO^+ data obtained in December 1995 and July 1996 do not show any residual (Fig. 8). Although the time span is only six months, the considerably higher quality of the data makes a comparison sensitive to very small changes in both the location of the absorption lines and their depths. The sensitivity for shifts in velocity is very good and the limits

are less than -0.2 to $+0.3\,\mathrm{km\,s^{-1}}$; The difference depends on the shape of the absorption profiles. This allows us to put an upper limit of 10% to changes in the HCO^+(1–0) absorption line in Cen A. If the molecular ISM in Cen A have small scale structures similar to those found in our Galaxy, this negative result implies that the background continuum source at millimeter wavelengths has an extent $\gtrsim$500 AU. The limit given by VLBI is 6000 AU. However, it should be kept in mind that if the absorbing gas is made up of a large number of small clouds (>200 per absorption feature) with angular extent smaller than that of the continuum source, changes will be difficult to detect since the clumps would tend to average out over time (e.g. Marscher & Stone 1994). Only future high–quality data can solve the question regarding variations in the absorbing gas in Cen A

4. Column densities and abundance ratios

4.1. Basic assumptions

In order to derive accurate column densities from the absorption lines, we have to make three assumptions. These are

1. assume a value for the covering factor f of the absorbing molecular gas with respect to the extent of the radio core in Cen A.
2. assume a value for the excitation temperature T_x of the absorbing gas.
3. assume that each molecular species is in local thermodynamical equilibrium, i.e. that all the rotational levels are characterized by the same excitation temperature (called then the rotational temperature T_rot).

The covering factor f is unknown for Cen A, but due to the small size of the radio core ($\lesssim$2.0 mas=6000 AU), it is likely to be close to unity for the molecular gas. Also, the extinction towards the core of Cen A at optical wavelengths has been estimated to be $A_\mathrm{V} = 15 \pm 5$ mag (Eckart et al. 1990), corresponding to a substantial amount of obscuring material. The depth of the deepest HCO^+(1-0) absorption line (no. 1 in Table 2) is 0.95 when the continuum level is unity. If the line is saturated, this means that 95% of the continuum source is covered by molecular gas. If, on the other hand, the absorption line is not saturated, the covering factor is larger. The abundance ratio of $HCO^+/H^{13}CO^+$ for the deepest absorption line is $\sim$70. This ratio would be lower than the real $^{12}C/^{13}C$ ratio if (1) the HCO^+ line was saturated and (2) if isotopic fractionation augments the $H^{13}CO^+$ abundance. The high $HCO^+/H^{13}CO^+$ ratio therefore shows that the HCO^+ line is unlikely to be strongly saturated. The nondetection of N_2H^+ is consistent with this scenario. The observed optical depth is nevertheless 3.0 for the deepest absorption component. The other absorption components are not as deep, but the upper limits to the $HCO^+/H^{13}CO^+$ ratio at

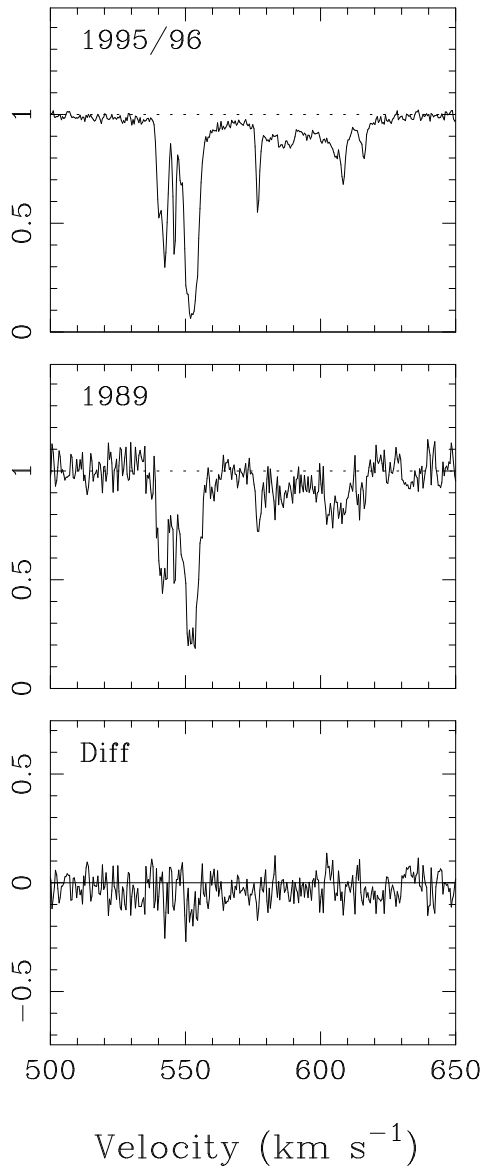

Fig. 7. HCO^+(1–0) spectra obtained in 1995/96 (present paper) and in 1989 (Eckart et al. 1990). The difference (1995/96 − 1989) is shown in the third panel. The spectra have been binned to a velocity resolution of 0.6 $\mathrm{km\,s^{-1}}$ before subtraction. No significant differences can be found.

Table 6. Column densities and abundance ratios for the main absorption components[a)].

Molecule	Low Velocity complex[b)]				Average LV[c)]	High Velocity complex
	1	2	3	4	1–4	5
	552.3 km s^{-1}	545.9 km s^{-1}	542.5 km s^{-1}	540.0 km s^{-1}	538–560 km s^{-1}	600.0 km s^{-1}
HCO^+	13.659	12.595	12.959	12.490	13.790	13.420
$H^{13}CO^+$	11.809	<10.615	<10.777	<10.657	11.916	11.821
HCN	13.424	12.745	12.756	12.689	13.683	13.187
HNC	12.883	12.280	12.150	11.851	13.099	12.851
CS	13.022	12.439	12.415	12.016	13.246	13.355
$\frac{HCO^+}{H^{13}CO^+}$	71	>96	>152	>64	75	>40
$\frac{HCO^+}{HCN}$	1.7	0.7	1.6	0.6	1.3	1.7
$\frac{HCO^+}{HNC}$	6.0	2.1	6.4	4.4	3.8	3.7
$\frac{HCO^+}{CS}$	4.3	1.4	3.5	3.0	3.5	1.2
$\frac{HCN}{HNC}$	3.5	2.9	4.0	6.9	3.8	2.2
$\frac{HCN}{CS}$	2.5	2.0	2.2	4.7	2.7	0.7
$\frac{HNC}{CS}$	0.7	0.7	0.5	0.7	0.7	0.3

a) An excitation temperature of 5 K has been used for all calculations.
b) The velocities are the average center velocities from all the molecules. Column densites are given as $\log(N/\mathrm{cm}^{-2})$.
c) For HCN the LV complex is defined by the velocity intervall 525–560 km s^{-1} due to the hyperfine components.

the corresponding velocities (Table 7) implies that these lines are not saturated and, hence, that their covering factors are always larger than their depth in the normalized spectra. In the following we will assume that $f = 1$.

The excitation temperature defines the relative population of two levels and can be derived if the velocity integrated optical depths of two rotational transitions of the same molecule can be determined. This is not the case for Cen A. Furthermore, in order to derive the total column density we must link the fractional level population to all the levels. This is done by invoking a weak LTE–approximation and assuming that $T_\mathrm{x} = T_\mathrm{rot}$, where T_rot is a temperature which governs the fractional population of all rotational levels in a given molecule. The LTE approximation is weak in the sense that it does not imply that T_rot equals the kinetic temperature and it allows for different molecules to have different T_rot. With this approximation we can use the partition function $Q(T_\mathrm{x})$ to express the total column density N_tot as

$$N_\mathrm{tot} = \frac{8\pi}{c^3}\frac{\nu^3}{g_J A_{J,J+1}} f(T_\mathrm{x}) \int \tau_\nu dV \ , \qquad (3)$$

where $\int \tau_\nu dV$ is the observed optical depth integrated over the line for a given transition, g_J the statistical weight for rotational level J, $A_{J,J+1}$ the Einstein radiative transition coefficient for levels J and $J+1$, and

$$f(T_\mathrm{x}) = \frac{Q(T_\mathrm{x})\exp(E_J/kT_\mathrm{x})}{1-\exp(-h\nu/kT_\mathrm{x})}. \qquad (4)$$

The excitation temperature is most likely low for the gas seen in absorption. The reason is that a high T_x quickly depopulates the lower rotational levels and decreases their opacity. For $T_\mathrm{x} \gtrsim 10\,\mathrm{K}$, $\int \tau_\nu dV \propto N/T_\mathrm{x}^2$. Hence, along a line of sight with a mixture of molecular gas components of similar column density but with different excitation temperatures, absorption lines of ground transitions will preferentially sample the excitationally coldest gas. Excitationally cold gas does not necessarily imply that the kinetic temperature is low. HCO^+, HCN and HNC are thermalized at H_2 densities of $10^5\,\mathrm{cm}^{-3}$. A molecular gas with densities lower than this would therefore give these molecules a low excitation temperature. In a survey of HCO^+(1–0) absorption and emission in our Galaxy, Lucas & Liszt (1996) find only one case out of eighteen where emission is associated with the absorption. This shows that the excitation temperature in the gas sampled through absorption is indeed very low. Also denser molecular gas seen in absorption has a low excitation temperature. Greaves & Williams (1992) measured T_x using CS(2–1) and CS(3–2) for several clouds towards Sgr B2 and found T_x to be always <4 K.

The detection of a relatively strong absorption of CS(2–1) does not necessarily imply either a high T_x or a high density. The J=1 level of CS has an energy corresponding to 2.35 K and should be significantly populated by the cosmic microwave background radiation. We searched for the CS(3–2) line and came up with a very weak detection of the main line at 552 km s^{-1} (line no. 1 in Table 2). The line is too weak to allow a determination of the excitation temperature, but the mere difficulty in detecting this line is a strong indication that the excitation temperature is low. The J=2 level of CS has an energy corresponding to 7.05 K. The CO molecule is detected in both the J=1–0, J=2–1 and J=3–2 transitions. The energy J=1 and J=2 levels correspond to temperatures of 5.53 and 16.6 K, respectively. The HV complex is tentatively detected in CO J=3–2 (Israel et al. 1991) [2]. CO has an electric dipole moment more than 10^3 times lower than either HCO^+, HCN, HNC and CS, and is thermalized at H_2 densities which are 10^2 times lower. Hence, the excitation temperature of CO is likely to be higher. This is consistent with the weak LTE assumption made above, where T_x can vary between different molecular species.

Since we have observed molecules with a large electric dipole moment, we will use $T_x = 5$ K for all the lines when deriving column densities. If the excitation temperature is close to the cosmic microwave background temperature, we overestimate the column densities of HCO^+, HCN and HNC by a factor 2.0. For CS the factor is 1.5. If, on the other hand, the excitation temperature is 10 K, we would underestimate the HCO^+, HCN and HNC column densities by a factor 3.1 and the CS by a factor 2.5.

A low T_x means that only the lowest rotational levels are significantly populated and that the assumption that one single temperature governs the overall population distribution, i.e. $T_x = T_{rot}$ is likely to be valid. The abundance ratios are very insensitive to the assumed excitation temperature, only depending on the weak LTE assumption. Hence, the column densities should be accurate to within a factor of 2, while the abundance ratios are very robust estimates.

4.2. Qualitative results

We calculated column densities for the four absorption lines in the LV complex by using the gaussian components given in Table 2. For the HV complex we derived the velocity integrated optical depth directly from the spectra[3].

[2] The HV is not visible in CO(1–0) with single dish telescopes, because of confusion with larger-scale emission. Interferometer CO(1–0) data obtained with the JCMT and CSO telescopes on Mauna Kea resolve out the emission component and the HV absorption components are obvious (JCMT Newsletter No. X).

[3] Only the HCO^+ spectrum gives values which are discrepant from the gaussian fits, due to the presence of several narrow absorption components in the HV complex.

Table 7. Column densities of HCO^+ in the High Velocity absorption complex

Comp.	Velocity[a] km s^{-1}	log N/cm^{-2}[b]
5a	574–580 km s^{-1}	12.621
5b	583–593 km s^{-1}	12.651
5c	598–612 km s^{-1}	12.912
5d	613–620 km s^{-1}	12.410

a) Velocity region over which the integrated opacity was obtained.
b)An excitation temperature of 5 K has been used for all calculations.

The results are presented in Table 6. For HCN we used the decomposition of the hyperfine components as given in Table 3. For all lines we used an excitation temperature of 5 K. Upper limits to the velocity integrated optical depth of $H^{13}CO^+$ was derived as

$$\int \tau_\nu dV \leq 3\sigma_\tau \sqrt{\Delta V \delta V} \ , \qquad (5)$$

where σ_τ is the rms of the opacity (0.012), δV the velocity resolution (0.15 km s^{-1}) and ΔV the assumed line width. For the latter we used 50% of the corresponding HCO+ line (compare with the line widths of HCO^+ and $H^{13}CO^+$ for line no. 1). A 3σ upper limit to the N_2H^+ column density, not given in Table 6, is 5.6×10^{12} cm^{-2}. This is derived in the same way as above, but with a ΔV of 5 km s^{-1} in order to compare it with line no. 1.

In Table 7 we present column densities and abundance ratios for 4 clearly defined HCO^+(1–0) components in the High Velocity complex. The components can only be identified in the HCO^+ spectrum and are designated 5a–d. They are defined in a smoothed spectrum and correspond to gaussian components 10, 11-13, 14–16 and 17 as given in Table 5. Integrated optical depths were derived by integrating over the velocity intervals given in Table 7.

5. Discussion

5.1. Type of molecular clouds

The column density of HCO^+ in Cen A ranges between 3.0×10^{12} cm^{-2} to 4.6×10^{13} cm^{-2} (Table 6). These column densities are all higher than the onset of CO self–shielding, which occurs at HCO^+ column densities $(1-3) \times 10^{12}$ cm^{-2}

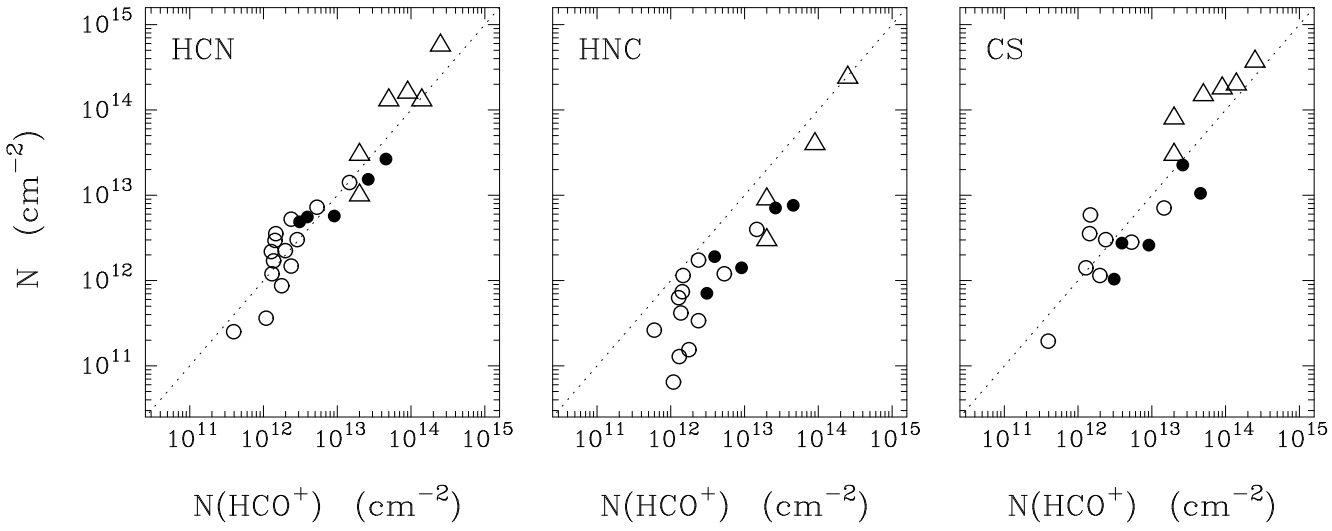

Fig. 9. HCO^+ column density vs. HCN, HNC and CS column density. Filled circles represent our data on Cen A, open circles data from Galactic diffuse clouds (Lucas & Liszt 1993, 1994, private communication) and triangles data towards SgrB2 from Greaves & Nyman (1996). The HCO^+ column densities of Lucas & Liszt have been multiplied by a factor 1.4 due to different use of the electric dipole moment. The dotted line represents a one–to–one correspondance between the column densities.

(Lucas & Liszt 1996). Hence the absorption in Cen A arises in gas which has a relatively low C^+/C ratio. If the gas in Cen A follows the same tight correlation between $N(HCO^+)$ and $N(OH)$ as Galactic clouds (Lucas & Liszt 1996), our HCO^+ measurement imply OH column densities in the range $(0.1-2)\times10^{15}\,\mathrm{cm}^{-2}$. These $N(OH)$ values are consistent with those inferred by van Langevelde et al. (1995) in Cen A.

In Fig. 9 we plot the column density of HCO^+ versus the column density of HCN, HNC and CS. We also include absorption line data from Galactic diffuse clouds obtained by Lucas & Liszt (1993, 1994, 1996) and somewhat denser clouds seen towards Sgr B2 (Greaves & Nyman 1996). The latter clouds are in some cases blended with gas close to the Galactic center. We have multiplied the HCO^+ column densities of Lucas & Liszt with a factor 1.4 in order to correct for the use of different values of the electric dipole moment. The dotted line in the figure is not a fit to the data but represents a one–to–one correspondance between the column densities. The gas in Cen A follows the same correlation as that of Galactic molecular gas. We have used an excitation temperature of 5 K when deriving column densities, while Lucas & Liszt and Greaves & Nyman have used 2.76 K. Since the molecules have almost exactly the same dependence on T_x, this has no influence on the result.

Although the excitation temperature is likely to be low in the molecular gas seen in absorption, the HCN/HNC ratios implies that the kinetic temperature is rather high. The formation of HCN and HNC depends on the gas temperature (cf. Irvine et al. 1987), with HCN preferentially being formed in warm gas on behalf of its isotopomer HNC. In the LV complex we find HCN/HNC ratios ranging between 3–7, while the HV complex has a ratio of 2.2. This gives a kinetic temperature of the LV complex of 20–30 K, while the HV gas is characterized by a kinetic temperature of $\lesssim$10 K.

A more detailed comparison of the 5 main absorption components as defined in Table 2 and 6, shows that component 1 and 3 (in the LV complex) shows similar behaviour in their abundance ratios (see Table 6). The differences between the components are, however, relatively small and do not show up as significant deviations in Fig. 9. The ratios of the hyperfine components of HCN (Table 4) indicate that component 1 and 3 are close to the LTE values; $R_{12}=0.6$, $R_{02}=0.2$, while component 2 and 4 deviates from LTE. Here we have to keep in mind that in the decomposition of the hyperfine lines some components suffer from near overlap and that the F=0–1 line of component 4 is an upper limit. Nevertheless, it is tantalizing that the two components with close to LTE ratios also show similar abundance ratios, while the other two components (plus the HV complex) differs by factors of 2–3 from each other. Anomalous excitation of the HCN hyperfine lines is often seen in Galactic molecular clouds (cf. Guilloteau & Baudry 1981, Walmsley et al. 1982), with the R_{12} ratio lower than LTE values in warm clouds and the R_{01} ratio lower than LTE values in cold clouds. In dense regions, where the HCN(1–0) line thermalizes, both ratios tend to unity. This latter case appears to be the case for component no. 2 in Cen A, at least for the R_{12} ratio.

In Fig. 10 we compare the HCO^+(1–0) spectrum with the HI absorption obtained with the VLA (van der Hulst et al. 1983). The HCO^+ spectrum has been binned to the same velocity resolution as the HI data, 6.2 km s^{-1}. A 3–component gaussian fit to the HCO^+ spectrum and

the residual is also shown. The appearance of the spectra agree quite well, even though the redshifted HCO^+ is more spread out in velocity than the HI. Column densities and N(HI)/N(HCO^+) ratios are given in Table 8. The component at $\sim$580 km s^{-1} appears to have a higher molecular gas fraction than the other two by a factor of $\sim$3.

In summary, all of the molecular gas components seen in absorption towards the nucleus of Cen A have a chemistry similar to that of Galactic diffuse molecular gas. Only the column densities are higher in Cen A than in typical Galactic diffuse clouds, which could be due to unresolved line components (i.e. more clouds) in the line of sight through the edge–on disk. The narrow HCO^+ lines seen in the HV complex reveal a relatively diffuse gas with lower abundances and a low kinetic temperature ($T_k \leq$ 10K).

Table 8. Column densities for HCO^+ and HI[a)].

Comp.[b)]		N(HCO^+)	N(HI)	N(HCO^+)/N(HI)
V(HCO^+)	V(HI)	cm^{-2}	cm^{-2}	10^{-8}
550	553	13.683	21.415	0.5
582	576	13.098	21.279	1.5
608	596	13.063	20.708	0.4

Column densites are given as $\log(N/\mathrm{cm}^{-2})$.
a) HCO^+ is smoothed to a velocity resolution of 6.2 km s^{-1}. Column densities for HI derived assuming T_s = 100 K.
b) Center velocities for the HCO^+ and HI lines (see Fig. 10).

5.2. Location of the absorbing molecular gas

The presence of two absorption complexes in Cen A, one at the systemic velocity and one redshifted relative to the systemic velocity, has led to speculations that the redshifted component arises in gas falling into the nucleus of Cen A, possibly feeding a supermassive black hole (cf. van der Hulst et al. 1983, van Gorkom et al. 1989). One argument is that the redshifted HI component is only seen towards the radio core and not against the inner jet (van der Hulst et al. 1983). The detection of λ2cm H_2CO in absorption against the inner jet (Seaquist & Bell 1990) is not necessarily a proof against the infall hypothesis, if the inner circumnuclear molecular disk is extended on scales of $\sim$300 pc. On the other hand, the lack of redshifted HI absorption against the inner jet could also mean that while the size of the HI component at the systemic velocity is $\gtrsim$300 pc (in order to cover both the jet and the core), the extent of the redshifted gas is smaller.

HI absorption has been detected in 9 elliptical galaxies (van Gorkom et al. 1989, Mirabel 1990 and references therein). In all cases the absorption is redshifted with respect to the systemic velocity. It is not clear whether this preponderance of redshifted absorption reflects a true infall of gas or if it results from a systematic offset in the systemic velocities towards the blue. Such systematic errors are known to exist due to outflow of emission line gas, which is often used to derive the systemic velocity. In spiral galaxies the situation is different. Here HI absorption is often seen as a single broad line, extending into both the blue– and redshifted sides around the systemic velocity (cf. Dickey 1986). With higher spatial resolution, the broad HI component is decomposed into a narrow one, shifting across the finite extent of the background radio source, over all velocities defined by the rotation of the disk (Koribalski et al. 1993). These absorptions originate in fast rotating circumnuclear disks or rings, of size $\sim$200 pc, and with velocities $\sim$200 km s^{-1} (e.g. NGC 253, 660, 1808, 3079, 4945, Milky Way).

The same phenomenon could be occuring in the center of Cen A, where the presence of a nuclear disk or ring of $\sim$100 pc radius and rotating with a velocity of $\sim$220 km s^{-1} has been established (Rydbeck et al. 1993). High rotational velocities at small galactocentric distances are naturally occuring in elliptical galaxies due to the high mass concentration towards the center (cf. Hernquist 1990) and non–circular orbits for the gas can be generated through non-axisymmetric gravitational instabilities (e.g. bar) or in the form of tri–axiality of the elliptical galaxy itself. Since the angular extent of the continuum source in Cen A is $\lesssim$2 mas (6000 AU), either blue or redshifted gas, depending on the orientation of the orbits, can be seen in absorption.

This situation is reminiscent of what happens in the center of the Milky Way. Here the velocities are more strongly non–circular, maybe because the central bar is oriented at 20–30° from the Sun line of sight (e.g. Blitz & Spergel 1991, Weinberg 1992). HCO^+ absorption in front of the central continuum source SgrA reveals a broad component between -210 to -110 kms, interpreted as coming from the $\sim$200 pc nuclear disk, and four narrower features (at -51, -30, -2 and $+32$ km s^{-1}) corresponding to known spiral arms in the galactic disk (Linke et al. 1981). The broad component at negative velocities is also seen in absorption in front of SgrB2, in HCO^+ as well as $H^{13}CO^+$ and HCN (Linke et al. 1981, Greaves & Nyman 1996). The size of the millimeter continuum source SgrA has recently been determined through VLBI at 3 and 7 mm (Krichbaum et al. 1994), and is 0.33 and 0.75 mas respectively. At those frequencies, the interstellar scattering becomes negligible, so these figures are believed to be the actual source sizes (Krichbaum et al. 1994). Since these source sizes correspond to $\sim$5 AU at the Galactic Center distance, the HCO^+ absorption features prove that the apparent line of sight velocity dispersion can be quite high in a typical edge–on nuclear disk, due to the accumulation on the line of sight of differential non–circular motions.

The emitting molecular gas in Cen A is confined to the center region, consisting of the nuclear disk or ring at a radius of ∼100 pc and an outer ring (or spiral arm) at ∼750 pc. The absorption complexes are likely to be associated with these features, but since absorption is sensitive to diffuse and low excitation molecular gas which is generally not seen in emission (e.g. Lucas & Liszt 1996), it is possible that some intervening molecular gas detected in absorption is associated with the larger HI disk extending to 7 kpc (Schiminovich et al 1994). As we have seen in the previous analysis, the molecular gas in both LV and HV components is diffuse, with abundance ratios similar to Galactic values. The main difference is that gas in the LV components has a higher kinetic temperature than the HV components. We cannot differentiate between inner and outer molecular gas from this alone. There are, however, two facts which suggest that the HV components are associated with the nuclear gas and the LV components with the outer disk: (1) the LV components are close to the systemic velocity and, (2) whereas the LV components extend between 540–556 km s^{-1}, the HV components are spread out between 576–640 km s^{-1}, ∼4 times larger. Although the rotational velocities are similar for the inner and outer molecular gas (Rydbeck et al. 1993), the inner region has a larger velocity gradient and this gas seen in absorption should be spread over a larger velocity interval.

The blue-shifted 'wing', from 500 to 540 km s^{-1}, has not been considered above. This feature is seen at a very low level, and depends on the subtracted emission profile shape, and should be viewed with caution. Could this gas comes from inside the cavity delineated by the circumnuclear ring? There is a constraint on the radius where molecules can subsist, around a luminous ionizing X–ray source. Maloney et al. (1994) derived an effective ionization parameter ξ_{eff}:

$$\xi_{eff} = 1.1 \times 10^{-2} L_{44}/(n_9 r_{pc}^2 N_{22}^{0.9})$$

where L_{44}= L$_x$/10^{44}erg s^{-1}, n_9 = n(H$_2$)/10^9 cm^{-3} and $r_{\rm pc}$ is the distance from the X–ray source in parsecs. The gas will not become substantially molecular unless the effective ionization parameter is smaller than 10^{-3}. From ROSAT HRI measurements, Döbereiner et al (1996) have estimated an X-ray luminosity (0.1-2.4 kev) for the Cen A nucleus of L$_{\rm x}$ = 3×10^{41} erg s^{-1} in 1994, after correcting for absorption. For diffuse gas with n(H$_2$)∼ 3×10^3 cm^{-3}, and a column density N(H$_2$) $\lesssim 10^{22}$ cm^{-2}, the minimum distance from the center is ∼100 pc. For molecular gas to exist at smaller galactocentric distances in Cen A, both the volume and column densities must be considerably higher. It is therefore likely that the molecular gas corresponding to the blue–shifted wing is at least at the distance of the circumnuclear ring. It is possible that this wing corresponds to the 750 pc component, which should also possess non–circular motions. The orientation of orbits in a tumbling non–axisymmetric component change by 90° at each resonance (e.g. Contopoulos & Grosbol 1989). Along the nucleus line of sight, it is therefore possible that this blue–shift component corresponds to elliptical streamlines perpendicular to that in the circumnuclear ring.

6. Summary

We have obtained new high signal–to–noise molecular absorption spectra towards the Centaurus A radio core. This has allowed the identification of up to 17 components in the HCO$^+$ spectrum. The components associated with the systemic velocity (LV) correspond to intervening material in the accreted gaseous disk of Cen A, well outside the circumnuclear ring in non–circular motions. It is not possible at present to derive their exact distances from the center. The high velocity (HV) redshifted components are interpreted in terms of a nuclear ring, at about 100 pc distance, with non–circular motions. The H^{13}CO$^+$ spectrum indicate that only the central component has relatively moderate opacities, while the HV components have low opacities. From the comparison between the HCO$^+$, HCN, HNC and CS spectra, we deduce that the absorbing gas is diffuse and cold on average. Abundances are compatible with Galactic values.

Comparison with the HCO$^+$ spectrum obtained 7 years ago by Eckart et al. (1990) revealed no time variations at a level >10%. Changes were expected from similar Galactic experiments. We therefore suggest that this constrains the apparent size of the mm continuum source to be larger than 500 AU (or ∼0.2mas), unless the absorbing gas is made up of a very large number of very small (a few tens of AU) clumps. In the latter case variations tend to average out over time. The core at 8.4 GHz appears as a point source ($\lesssim$2mas) in VLBI experiments (Jones et al. 1996). The source size is therefore constrained between 0.2 and 2 mas. The larger size might be only apparent, enlarged through interstellar scattering by the ionised gas in Cen A itself.

Acknowledgements. We thank R. Lucas and H. Liszt for communicating Galactic column density data prior to publication. TW acknowledges support from the Swedish Natural Science Council (NFR) for this research.

References

Blitz L., Spergel D.N. 1991, ApJ 379, 631
Combes, F., Wiklind, T. 1996, in Cold Gas at High Redshift, eds. M.N. Bremer, P. van der Werf, H.J.A. Röttgering, C.L. Carilli, Kluwer Academic Pub., p. 215
Contopoulos, G., Grosbol, P. 1989, A& AR 1, 261
Diamond P.J., Goss W.M., Romney J.D. et al. 1989, ApJ 347, 302
Dickey, J.M. 1986, ApJ 300, 190
Döbereiner S., Junkes N., Wagner S.J. et al. 1996, ApJ 470, L15

Eckart, A., Cameron, M., Genzel, R., Jackson, J.M., Rothermel, H., Stutzki, J., Rydbeck, G., Wiklind, T. 1990, ApJ 365, 522
Falgarone E., Puget J-L., Pérault M. 1992, A&A 257, 715
Frail D.A., Weisberg J.M., Cordes J.M., Mathers C.: 1994, ApJ 436, 144
Gardner, F.F., Whiteoak, J.B. 1976, MNRAS 175, L9
Greaves, J.S., Nyman, L.–Å. 1996, A&A 305, 950
Greaves, J.S., Williams, P.G. 1992, A&A 290, 259
Guilloteau, S., Baudry, A. 1981, A&A 97, 213
Hawarden, T.G., Sandell, G., Matthews, H.E., Friberg, P., Watt, G.D., Smith, P.A. 1993, MNRAS 260, 844
Hernquist, L. 1990, ApJ 356, 359
Irvine, W.M., Goldsmith, P.F., Hjalmarson, Å. 1987, in Interstellar Processes, eds. D.J. Hollenbach, H.A. Thronson, Reidel Publ. Co., p. 561
Israel, F.P. 1992, A&A 265, 487
Israel, F.P., van Dishoeck, E.F., Baas, F., de Graauw, T., Phillips, T.G. 1991, A&A 245, L13
Israel, F.P., van Dishoeck, E.F., Baas, F., Koorneef, J., Black, J.H., de Graauw, T. 1990, A&A 227, 342
Jones D.L., Tingay S.J., Murphy D.W. et al. 1996, ApJ 466, L63
Kellerman, K.I. 1974, ApJ 194, L135
Koribalski, B., Dickey J.M., Mebold U. 1993, ApJ 402, L41
Krichbaum T.P., Schalinski C.J., Witzel A. et al. 1994, in "The Nuclei of Normal Galaxies", ed. R. Genzel & A.I. Harris, Kluwer, Holland, p. 411
Linke R.A., Stark A.A., Frerking M.A.: 1981, ApJ 243, 147
Lovas, F.J. 1992, J. Phys. Chem. Ref. Data 21, 181
Lucas, R., Liszt, H. 1996, A&A 307, 237
Lucas, R., Liszt, H. 1994, A&A 282, L5
Lucas, R., Liszt, H. 1993, A&A 276, L33
Maloney, P.R., Begelman, M.C., Rees, M.J. 1994, ApJ 432, 606
Marscher, A.P., Moore, E.M., Bania, T.M. 1993, ApJ 419, L101
Marscher A.P., Stone A.L.: 1994, ApJ 433, 705
Mirabel, I.F. 1990, ApJ 352, L37
Moore, E.M., Marscher, A.P. 1995, ApJ 452, 671
Nicholson, R.A., Bland–Hawthorne, J., taylor, K. 1992, ApJ 387, 503
Quillen, A.C., de Zeeuw, P.T., Phinney, E.S., Phillips, T.G. 1992, ApJ 391, 121
Rydbeck, G., Wiklind, T., Cameron, M., Wild, W., Eckart, A., Genzel, R., Rothermel, H. 1993, A&A 270, L13
Schiminovich D., van Gorkom J.H., van der Hulst J.M., Kasow S. 1994, ApJ 423, L101
Seaquist, E.R., Bell, M.B. 1990, ApJ 364, 94
Tornikoski, M., Valtaoja, E., Teresranta, H., Karlamaa, K., Lainela, M., Nilsson, K., Kotilainen, J., Laine, S., Lahteemaki, A. et al. 1996, A&AS 116, 157
van der Hulst, J.M., Golisch, W.F., Haschick, A.D. 1983, ApJ 264, L37
van Gorkom, J.H., van der Hulst, J.M., Haschick, A.D., Tubbs, A.D. 1990, AJ 99, 1781
van Gorkom, J.H., Knapp, G.R., Ekers, R.D., Ekers, D.D., Laing, R.A., Polk, K.S. 1989, AJ 97, 708
van Langevelde, H.J., van Dishoeck, E.W., Sevenster, M.N., Israel, F.P. 1995, ApJ 448, L123
Walmsley, C.M., Churchwell, E., Nash, A., Fitzpatrick, E. 1982, ApJ 258, L75
Weinberg M.D.: 1992, ApJ 384, 81
Wiklind, T., Combes, F. 1996a, A&A 315, 86
Wiklind, T., Combes, F. 1996b, Nature, 379, 139
Wiklind, T., Combes, F. 1995, A&A 299, 382
Wild, W., Eckart, A., Wiklind, T. 1997, A&A submitted
Wilson T.L., Walmsley C.M. 1989, A&AR 1, 141

This article was processed by the author using Springer-Verlag LaTeX A&A style file *L-AA* version 3.

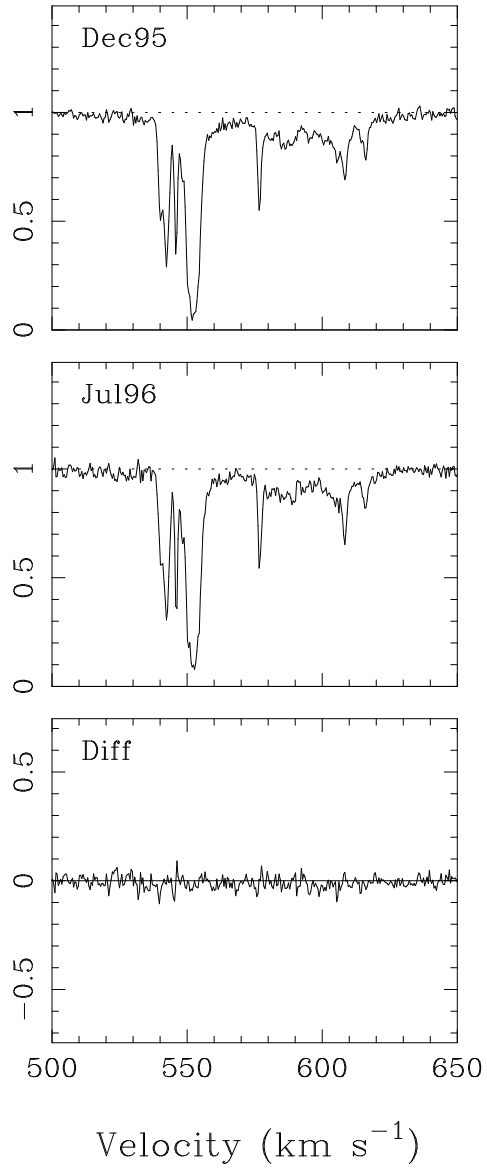

Fig. 8. HCO^+(1–0) spectra obtained in December 1995 and in July 1996. The difference is shown in the third panel. The spectra have been binned to a velocity resolution of $0.6\,\mathrm{km\,s^{-1}}$ before subtraction. No differences can be found.

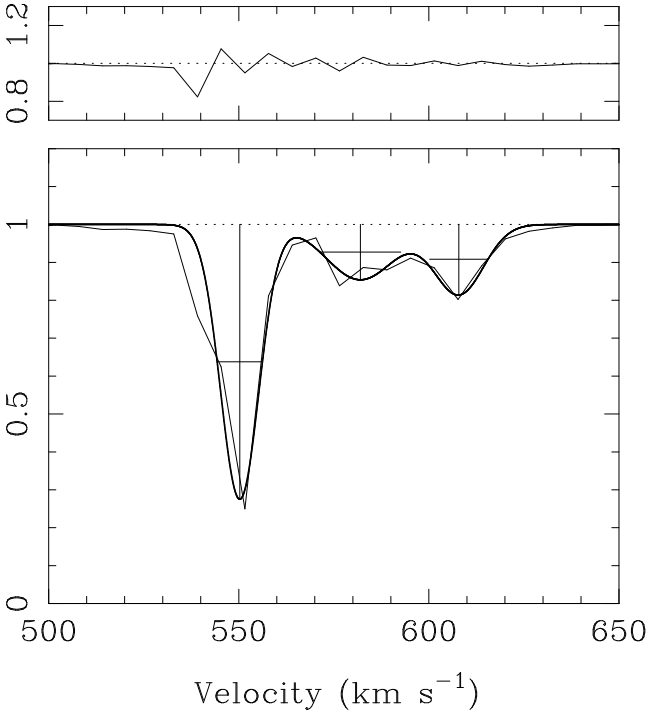

Fig. 10. The HCO^+(1–0) spectrum binned to a velocity resolution of $6.2\,\mathrm{km\,s^{-1}}$, which is the same as the 21cm HI spectrum obtained by van der Hulst et al. (1983). Also shown is a 3–component gaussian fit and the residual spectrum.